communications chemistry

A Nature Portfolio journal

Article

https://doi.org/10.1038/s42004-025-01757-y

Crystalline polymeric phases of sulphur dioxide

Huichao Zhang[1], Philip Dalladay-Simpson[1] ✉, Francesco Capitani[2], Cheng Ji[1,3], Li Zhang[1], Mario Santoro[4,5] ✉, Federico A. Gorelli[1,3,4,5] ✉ & Roman Martoňák[6] ✉

SO_2 is a molecule of significant industrial and geochemical importance, known for its role in sulphuric acid production and its natural occurrence in volcanic processes. Recent studies have revealed pressure-induced amorphisation and the formation of polymeric amorphous phases in SO_2, behaviours analogous to those observed in other fundamental molecular systems such as CO_2, N_2, and CS_2. Here, we identify a mixture of polymeric SO_2 phases, with space groups *Ama*2 ($Z = 2$) and $Pmc2_1$ ($Z = 8$), the latter a homologue of γ-SeO_2, as the crystalline parents of the previously reported threefold-coordinated amorphous SO_2 observed above 25 GPa. These phases were characterized using a combination of advanced synthesis and refined high-pressure loading techniques, alongside x-ray diffraction, Raman, and infrared spectroscopy. Structural assignments were further supported by numerical predictions of candidate crystal structures. Notably, the *Ama*2 and γ-SeO_2-like phases exhibit in the pressure region 20–60 GPa the lowest and near-degenerate enthalpies, *Ama*2 being stable below 25 GPa and γ-SeO_2-like above 25 GPa. Both phases feature distinctive W-shaped polymeric units, a structural motif identified long ago at ambient pressure in the rare-mineral Downeyite (SeO_2), but the stacking of chains is different and pressure-dependent.

Polymers, large macromolecules composed of repeating molecular units, are integral to modern society, with applications spanning industry, biomedicine, and emerging technologies such as fused deposition modelling in 3D printing. Their versatility stems from tunable physical properties such as elasticity, optical behaviour, and thermal and chemical stability. Polymerisation can occur under diverse conditions, with the constituent elements of sulphur dioxide (SO_2) serving as an excellent example. Sulphur (S) readily polymerizes at ambient pressure requiring temperatures of only 160 °C (λ-transition) to open the S_8 molecular rings and form long polymeric-chains[1,2]. Molecular oxygen (O_2) on the other hand is expected to polymerize only at extreme densities, theoretically requiring pressures in excess of 1.9 TPa to break the oxygen double-bond and make square-spiral-like polymeric chains[3]. In between these two examples, high-pressure environments generated by diamond anvil cells (DACs) have proven to be a unique tool to generate new exotic density-stabilized polymers. Many examples of high-pressure polymers have been observed experimentally and predicted theoretically in systems such as N_2[4–11], CO[12–16], CO_2[17–20], CS_2[21–26], and benzene[27,28]. Interestingly, depending on temperature, polymerisation can occur in the solid phase, forming chains[29], layers[30] or covalent networks[8,31], or in the liquid phase, where polymeric liquids may emerge via liquid-liquid phase transitions[1,2]. Additionally, the process of polymerisation under high pressure can often result in amorphous "glass-like" phases, as demonstrated in systems such as N_2[7,31], CO_2[32] and SO_2[33]. Although these non-equilibrium systems reveal fascinating physics and hold potential geological relevance, probing the atomistic nature of these amorphous polymeric states can be challenging. This is because symmetry-probing techniques, such as vibrational spectroscopy and diffraction, often produce weak, broad, and complex responses. However, the polymeric crystalline parent structures, which provide accessible atomistic information and are the thermodynamically stable phases for the substances undergoing polymerization, can be obtained by applying extreme temperatures, typically higher than 1000 K, although this has been achieved so far only in very few cases such as for CO_2 and N_2[19,20,31].

SO_2 is a simple molecule of considerable importance in chemistry, industry, geochemistry and planetary science. It is found on Earth, Mars, and Venus, where its primary source is thought to be volcanic activity and

[1]Center for High Pressure Science and Technology Advanced Research, Shanghai, China. [2]SOLEIL, L'Orme des Merisiers Départementale 128, Saint-Aubin, France. [3]Shanghai Advanced Research in Physical Sciences (SHARPS), Shanghai, China. [4]Instituto Nazionale di Ottica, Consiglio Nazionale delle Ricerche (CNR-INO), Sesto Fiorentino, Italy. [5]European Laboratory for Non Linear Spectroscopy (LENS), Sesto Fiorentino, Italy. [6]Faculty of Mathematics, Physics and Informatics, Department of Experimental Physics, Comenius University, Bratislava, Slovakia. ✉e-mail: philip.dalladay-simpson@hpstar.ac.cn; santoro@lens.unifi.it; federico.gorelli@hpstar.ac.cn; martonak@fmph.uniba.sk

also human-caused pollution on Earth, and it exists on the moons of Jupiter. On Venus, SO_2 is the third most abundant atmospheric gas and a key component of the planet's atmospheric sulfur cycle[34]. Also, sulfur dioxide was a key agent in the warming of early Mars. Despite the importance of this substance and extensive research on high-pressure polymerizations, the polymerization of SO_2 remains poorly understood. At ambient pressure, SO_2 crystallizes into an orthorhombic structure at 143 K[35], where the molecules are orientationally ordered with the molecular planes parallel to the c-axis. Additionally, two high-pressure molecular phases, denoted as SO_2-II and SO_2-III, have been observed demonstrating the stability of the molecule to at least ~7.5 GPa[36]. Several more recent DAC experiments at higher pressures have unveiled dramatic changes in the bonding characteristics of SO_2, indicating the onset of polymerisation. Notably, Song et al. first reported evidence of an extended solid at 17.5 GPa and room temperature, revealing a substantial modification in the Raman spectrum, which they attributed to the formation of $(SO_2)_3$ clusters[37]. Subsequent work by Zhang et al. demonstrated that at slightly higher pressures, 26 GPa, a reversible transition between molecular and polymeric amorphous SO_2 occurs, showcasing a new example of polyamorphism[33], a finding confirmed by Raman and infrared spectroscopy, and X-ray diffraction. In the most recent study, Lu et al.[38] reported a molecular-to-polymeric transition around 21 GPa which remained relatively crystalline, with the structure tentatively assigned to the predicted $Pmc2_1$ ($Z = 4$) candidate model based on its qualitative compatibility with Raman spectroscopy. However, the propensity of SO_2 to amorphize during polymerisation has led to significant degradation in peak-shape observed in both diffraction and vibrational spectroscopy across all measurements to date, leaving a comprehensive characterization of its polymeric form challenging and largely unexplored.

In this study, we present a combined experimental and theoretical approach to determine the crystal structure of polymeric SO_2. Using advanced synthesis techniques, we produced crystalline polymeric SO_2 via two methods: cryogenic loading (Method I) and direct synthesis from a sulphur and O_2/He gas mixture (Method II), with the latter yielding superior polymeric crystallinity. The polymeric nature of SO_2 was characterized using powder X-ray diffraction, Raman, and infrared spectroscopy, revealing the onset of polymerisation around 21 GPa, consistent with previous studies[38], and showing recovery to pressures as low as 17 GPa. Crystal structure search methods and metadynamics identified four energetically most favourable candidate polymeric structures, with space groups $Pmc2_1$ ($Z = 8$, γ-SeO_2-like), $Ama2$, $Pmc2_1$ ($Z = 4$, β-SeO_2-like) and Pm, with extremely similar enthalpies (within few meV per formula unit (f.u.)). All these structures feature W-shaped polymeric SO_2 chains, a conformation previously seen at ambient pressure in the rare-mineral Downeyite (SeO_2)[29,39], however, with a quite different packing. Moreover, we found a $Pbcm$ phase which also has W-shaped chains and enthalpy higher by few tens of meV per f.u. and a distinct polymorph ($P2_1/c$) with U-shaped chain conformation and enthalpy higher by about 0.1 eV per f.u.. The latter conformation might be potentially inducible, e.g., by photoexcitation processes. The implications of this study are twofold: firstly, the characterization of this simple polymer at high density, which besides fundamental interest holds potential applications in geological models; and secondly, presenting a methodology for synthesizing highly crystalline polymers under high-pressure conditions, previously attainable only through extreme temperatures.

Results and discussion

SO_2 polymerisation identified via Raman and IR spectroscopy

In fig. 1, we present selected Raman spectra measured upon increasing (a, b) and decreasing (c) pressure, at room temperature, for a cryogenically loaded homogeneous sample (a) and for a sample obtained via direct synthesis

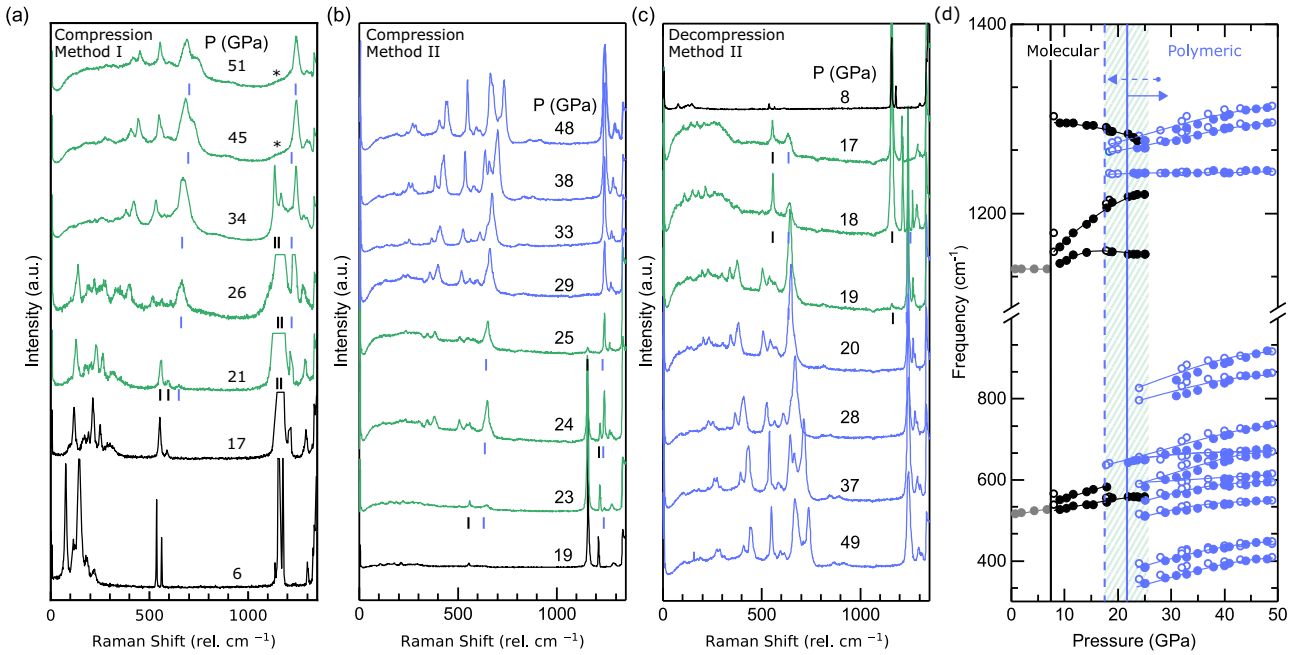

Fig. 1 | Raman spectroscopy of the pressure-induced polymerisation of SO_2. a SO_2 (Method I) on compression up to 51 GPa, black and blue ticks denote prominent vibrational modes from molecular and polymeric SO_2 in the green spectra, respectively. At 45 GPa and 51 GPa the asterisk denotes a weak feature of remanent amorphous molecular SO_2. **b**–**d** are Raman measurements on SO_2 synthesized from S in an O_2-He mixture (Method II). **b** Spectra with increasing pressure and (**c**) on decompression at room temperature. Trace colours indicate the states of SO_2: molecular (black), molecular-polymeric mixed (green), and polymeric (blue). In (**a**–**c**), all spectra are compared on the same scale at different pressures, except for being vertically offset. At the lowest pressures, in (**b**, **c**), the Raman peaks are very weak below 1000 cm^{-1}. **d** Pressure dependence of Raman-active vibrational modes of SO_2 in the selected frequency region of 300–1400 cm^{-1}; solid and empty symbols represent measurements on compression and decompression, respectively. Marker colours correspond to the states of SO_2 as depicted in (**a**–**c**). The blue vertical lines demonstrate the hysteresis of polymer formation, showing the onset of polymerisation upon compression (solid line) and the stability of the polymers upon decompression (dashed line). The green hatched area represents the range of coexistence between the molecular and polymeric phases observed during compression and decompression.

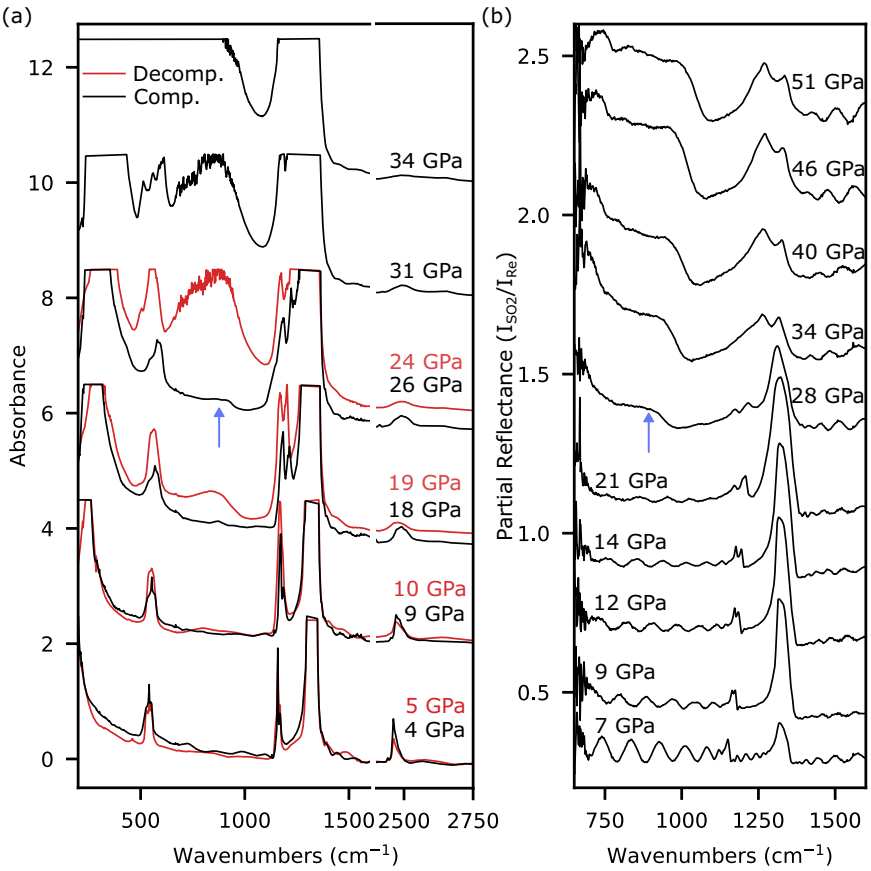

Fig. 2 | Infrared spectroscopy of the pressure-induced polymerisation of SO_2. a Synchrotron mid- and far-infrared absorption spectra of SO_2 measured up to 34 GPa during compression (black traces) and decompression (red traces). Above 34 GPa, no transmission is detected below 1400 cm^{-1}, resulting in saturated absorption. Compression and decompression traces are overlapped to highlight the strong hysteresis associated with the formation of polymers. **b** Mid-infrared reflectivity measurements conducted up to 54 GPa on compression. In both panels, a key vibrational feature, marked by the blue arrow, indicates the onset of polymerisation on compression.

from the elements (b and c) in He resulting in SO_2 crystals in He as the pressure transmitting medium (see Methods section). All spectra exhibit sharp peaks up to the highest investigated pressures of 48–51 GPa, demonstrating that the two samples are crystalline. In particular, for the homogeneous sample, we note that amorphisation was substantially prevented, at variance with our previous study[33], thanks to the much smaller gasket hole and to the fact that the gasket material was rhenium instead of the much softer stainless steel, which in turn reduced the shear stress. Nevertheless, a weak and broad band centered at around 1200 cm^{-1} at 45–51 GPa and highlighted by asterisks, show traces of the molecular amorphous form. On the other hand, no traces of amorphous material are observed in the sample in He, the peaks of which are sharper than those of the homogeneous sample, indicating a higher crystalline quality. The pressure evolution of the spectra for the two samples closely mirrors that of our recent study, where we observed the high-pressure transformation of SO_2 into an amorphous polymer, above 26 GPa[33], and can be interpreted similarly. We point out that this resemblance is limited to the frequencies and relative intensities, while the peaks of amorphous SO_2 were significantly broader as compared to those of the crystalline samples, due to disorder (see Fig. S1). We recall that the polymer was shown to be made of sulphur in three-fold coordination by oxygen, whereas oxygen was of two types: two-fold and singly coordinated by sulphur bridging (O_B) and terminal (O_T) oxygen, respectively, giving rise to single S-O_B and double bonds S=O_T. If we now focus on the homogeneous sample, we see that the spectra at 6 GPa and 17 GPa are those of the molecular solid. These spectra exhibit four distinct frequency regions, i.e., the lattice region below 400 cm^{-1}, the O=S=O bending at 500–600 cm^{-1}, the O=S=O symmetric stretching at 1100–1240 cm^{-1}, and the O=S=O asymmetric stretching at 1240–1320 cm^{-1}. At 21 GPa a major transformation, in fact polymerisation starts to appear and proceeds further upon increasing pressure. Progressively, the molecular peaks vanish and are substituted by polymeric peaks: S=O_T bond stretching peaks at 1200–1300 cm^{-1}, and several peaks at 300–1000 cm^{-1} which we attribute to the S-O_B bond stretching and to bending modes. However, the SO_2 molecular crystal is still observed well beyond the polymerisation pressure threshold up to at least 34 GPa, and the residual amorphous molecular form is observed at even higher pressures. For the sample in He, the polymerisation is much more sharp, as it starts at about 23 GPa, upon increasing pressure, and is complete above 25 GPa, leaving no traces of molecular materials. For this sample, we also checked reversibility. In fact, upon decreasing pressure, the transformation from the polymeric phase to the molecular solid begins at 19 GPa and is completed at 17 GPa. In panel (d) of Fig. 1, we report pressure shift of the peak frequencies of molecular and polymeric SO_2 for the sample in He. The total range of coexistence between the molecular and polymeric phases observed during compression and decompression is highlighted.

In Fig. 2(a), we report synchrotron mid- and far-infrared absorption spectra of a homogeneous SO_2 sample (Method I) measured up to 34 GPa, as a complement to the Raman investigation. Upon increasing pressure, at 4, 9 and 18 GPa, we observe the spectrum of the molecular solid, which exhibits saturated lattice peaks below 400 cm^{-1}, the O=S=O bending peak at 500–600 cm^{-1} and the O=S=O symmetric stretching peak at 1100–1240 cm^{-1}, both showing some crystalline splitting, the strong saturating O=S=O asymmetric stretching peak at 1240–1320 cm^{-1} and the overtone of this mode at about 2480 cm^{-1}. Between 18 and 26 GPa, a new band appears at around 800 cm^{-1} and rapidly intensifies further increasing the pressure. This band is entirely of non-molecular origin, and corresponds to the weak peaks observed in the Raman spectra of polymeric SO_2 in the same frequency range, strongly indicating that it arises from vibrational modes of the polymer. At 34 GPa, the absorption is saturated below 1400 cm^{-1}, except in the narrow 900–1150 cm^{-1} frequency range. On further compression the spectrum becomes fully saturated, allowing no detectable transmission from 1400 cm^{-1} down to the far-infrared region. Upon decreasing pressure, the IR transmission and absorption is recovered and the spectra clearly demonstrate the reversibility of the monomer-to-

polymer transformation, albeit with a strong hysteresis. To overcome the limitation due to IR absorbance saturation and gain more information from IR spectroscopy, we also measured in-house IR reflectivity spectra in the medium IR frequency range (Fig. 2(b)), upon increasing pressure. In these spectra, at 7–21 GPa, we see the molecular O=S=O symmetric and anti-symmetric stretching peaks at 1100–1240 cm^{-1} and 1240–1320 cm^{-1}, respectively. At 28 GPa, we observe the emergence of a new band at about 880 cm^{-1}, which corresponds to similar peaks in the IR absorption and Raman spectra and, consistently, we assign this band to polymeric modes. This band intensifies with pressure indicating that polymerisation proceeds further on compression. In addition, similar to the Raman spectra of the homogeneous sample, Fig. 1(a), the molecular stretching peaks are progressively substituted by a polymeric S=O_T stretching peak centered at about 1270 cm^{-1}, above 28 GPa.

More quantitative insight into the structure of polymeric SO_2 can now be given using structure search and DFT simulations, the results of which will be compared to the experimental results.

Polymeric SO_2 crystal structure search

To our knowledge, the structure of the crystalline polymeric phases of SO_2 have not yet been determined experimentally. An evolutionary structural search was previously conducted by the authors of this study within the framework of four SO_2 formula units at pressures of 10, 20, and 50 GPa[33]. In all identified polymeric structures, sulphur atoms are coordinated in a 3-fold manner by oxygen atoms, while half of the oxygen atoms are 2-fold coordinated by sulphur, and the remaining half are bonded to a single sulphur atom. The search revealed two optimal and nearly degenerate structures, $Pmc2_1$ ($Z = 4$) and *Ama*2, which are found to be stable at pressures exceeding 11 GPa compared to molecular SO_2 phases. The same $Pmc2_1$ ($Z = 4$) structure was also subsequently reported by Lu et al. and tentatively assigned to the extended phase of SO_2 at pressures above ~20 GPa[38]. We note that this predicted structure is the same as the β-SeO_2 polymorph, stable in SeO_2 above 2 GPa and below 600 K[40].

The energetically favourable phases, $Pmc2_1$ and *Ama*2, are different packing arrangements of identical polymeric strings consisting of corner-connected pyramidal entities, with sulphur atoms at their apex. An example of this arrangement can be seen in the various polymeric projections illustrated in Fig. 3(a). The unconnected corners of the pyramids result in a sulphur-oxygen double-bond (S=O) and referred to as terminal-oxygens (O_T). In contrast, the connections between the pyramidal entities are formed through S-O-S single bonds, identified as bridging-oxygens (O_B). This distinct and characteristic bonding arrangement compared with molecular SO_2, particularly the presence of singly-bonded O_B connections (mode frequencies at 500–900 cm^{-1}), leads to a significantly modified vibrational spectrum, as observed experimentally and discussed in detail in the previous section. Interestingly, when viewed along the chain axis, a characteristic W-shape emerges, highlighted by the green trace in Fig. 3(a), and is used to characterize the conformation of the polymer. The near-degenerate structures $Pmc2_1$ and *Ama*2 from our structural searches are shown in Fig. 3(b, c), respectively.

In order to identify further low-lying polymorphs at high pressure, possibly with more complex structural motifs we performed more extensive structural searches of crystalline phases of SO_2 employing the random search approach[41] and the PBE functional[42] (See "Methods" section for technical details). A search in the space of 4 SO_2 molecules was first performed at a simulation pressure of 38 GPa. The above mentioned $Pmc2_1$ and *Ama*2 structures were again found to be the most energetically competitive with near-degenerate enthalpies (~10 meV per f.u.), similar to what was reported previously[33]. Additional low-lying metastable structures were also identified; the *Pbcm* structure with enthalpy higher by 47 meV per f.u. and the $P2_1/c$ structure with enthalpy higher by 91 meV per f.u. with respect to $Pmc2_1$. All four structures are shown in Fig. S2 where it can be seen that while the *Pbcm* structure also consists of W-shaped polymers, the chains in $P2_1/c$ adopt a different conformation and have a characteristic U-shape.

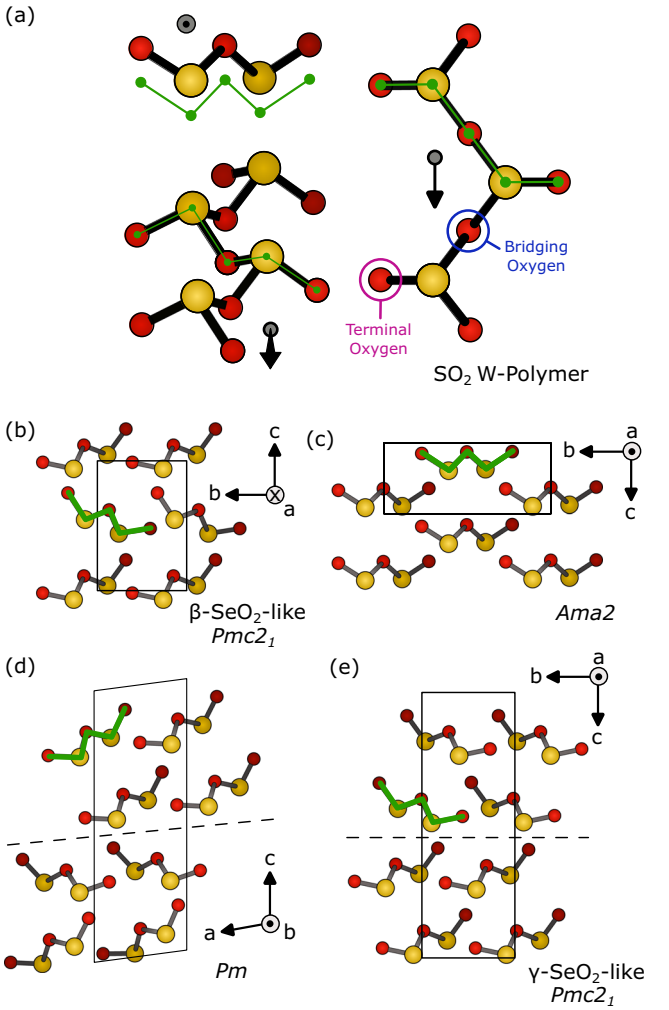

Fig. 3 | Candidate SO_2 W-polymer and associated crystalline structures identified through a random structure search at 38 GPa. a Various projections of the W-shaped polymeric chains are shown, with the arrows indicating their orientation. The green trace is used to visually highlight the W-shape. Candidate crystalline polymeric arrangements are illustrated in (**b**, **c**) for $Pmc2_1$ and *Ama*2, respectively. The *a*-axes of the unit cells for these structures, which are collinear with the polymeric chain, are oriented so that the propagation of the polymeric chain is perpendicular to the page. **d** Mixed structure, representing combination of $Pmc2_1$ and *Ama*2, found from random structure searches initiated using 8 SO_2 molecules. **e** A metadynamics simulation initiated from (**d**) resulting in interfaced *Ama*2 domains. In (**d**, **e**), a dashed line is used to identify an interface between the smaller $Pmc2_1$ and *Ama*2 domains.

In order to find other low-enthalpy structures with larger unit cells we performed also an additional random search in the space of 8 SO_2 molecules at pressure of 38 GPa. Among the low-lying structures we found a structure consisting of W-shaped chains which appears very similar to the $Pmc2_1$, but it contains a stacking fault (Fig. 3(d). In fact, this structure can be interpreted as a mixture of $Pmc2_1$ and *Ama*2, with the corresponding interface highlighted in Fig. 3(d) by a dashed line. This structure has a space group *Pm* and an enthalpy marginally higher than the $Pmc2_1$ by about 3.8 meV per f.u., being actually more energetically competitive than pure *Ama*2. In order to find other possible configurations of this kind we performed metadynamics simulations[43,44] starting from this structure, aimed at finding possible structural transitions to new structures of similar character. In this manner we obtained another low-enthalpy structure (Fig.3(e)) resulting from a transition where one layer of chains changed orientation. This structure can be interpreted as representing two grains of *Ama*2 interfaced by a stacking fault, highlighted by a dashed line Fig. 3(e), and is extremely energetically

competitive with an enthalpy only 2.1 meV per f.u. above the $Pmc2_1$ ($Z = 4$) phase. It has a space group $Pmc2_1$ ($Z = 8$) and corresponds to the γ-SeO_2 polymorph, stable above 6 GPa and above 600 K[40].

These findings strongly suggest that the structures $Pmc2_1$ ($Z = 4$) and *Ama*2 with W-shaped chains, differing only in chain packing, represent members of a larger class of more complex polytypes with very similar enthalpies. These could be formed from the *Ama*2 by introducing stacking faults with a different orientation of chains in the adjacent planes. In addition, metastable structures with higher enthalpy may be formed from stacking of chains with different conformation such as, e.g., the $P2_1/c$ structure with U-shaped chains.

Since the enthalpies of the four polymeric phases with W-shaped chains were found to be very close within the PBE functional, a proper assessment of their thermodynamic stability requires including also the van der Waals interaction which is critically important for packing of molecular units in such systems. However, this interaction is not well described by local DFT functionals such as PBE. We recalculated the enthalpy of all above mentioned phases in the pressure range from 20 to 60 GPa employing the highly accurate r^{2}SCAN+rVV10[45] functional which is recommended for description of structure and thermodynamics of layered solids[46]. The results are shown in Fig. 4. The enthalpies of the phases with W-shaped chains (except for the *Pbcm*) are still near-degenerate (within 10 meV per f.u.) in the whole pressure region. The other two phases, *Pbcm* with W-shaped chains and $P2_1/c$ with U-shaped chains are considerably higher and only metastable in the whole region. At 20 GPa, the *Ama*2 phase has the lowest enthalpy while at 25 GPa it is replaced by the γ-SeO_2-like polymorph which remains the most stable one up to 60 GPa. Beyond 60 GPa, it is likely that the β-SeO_2-like phase would become stable, however, in this region of pressures SO_2 was found to decompose in ref. 38. The calculations therefore predict a 1st order structural transition at 25 GPa between two polymeric phases, *Ama*2 and $Pmc2_1$ ($Z = 8$, γ-SeO_2-like) which both consist of the same W-shaped chains but differ in their packing. The pressure evolution of the most stable structure can be rationalized by noting that in the *Ama*2, stable at lower pressures, all chains have the same orientation. Upon increasing pressure, the system progressively forms stacking faults which allow a more efficient packing and decrease the volume, first every two layers in the γ-SeO_2-like phase and upon further compression every layer in the β-SeO_2-like phase. We note that we provide here a prediction for the most stable phase that is different from previous works[33,38] which considered only phases with $Z = 4$ and consequently overlooked the γ-SeO_2-like phase.

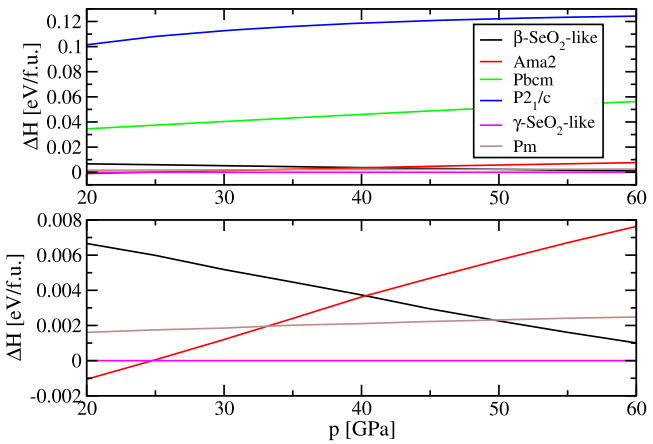

Fig. 4 | Relative enthalpies for candidate structures for polymeric SO_2. Upper panel: Pressure dependence of the enthalpies of the phases β-SeO_2-like, *Ama*2, *Pbcm*, $P2_1/c$, γ-SeO_2-like and *Pm* in the pressure range from 20 to 60 GPa. The enthalpies were calculated with the r^{2}SCAN+rVV10[45] functional and are relative to the γ-SeO_2-like phase. Lower panel: Enthalpies of the four lowest enthalpy phases which are very similar in structure, enthalpy and volume, shown on an order of magnitude smaller enthalpy scale.

Crystallographic Information Files (CIF) calculated at 55 GPa for the six predicted structures: $Pmc2_1$ ($Z = 8$, γ-SeO_2-like), *Ama*2, $P2_1/c$, $Pmc2_1$ ($Z = 4$, β-SeO_2-like), *Pbcm* and *Pm* are available as Supplementary Data 1–6, respectively.

To close this section, we comment about the applicability of the pressure homology rule to the analogy between SO_2 and SeO_2. According to this rule, the SeO_2 structures at low pressures should be similar to the SO_2 structures at high pressure. The structure of a polymeric phase is determined both by the chain conformation and their stacking. Concerning the conformation, the W-shaped chains found in SeO_2 in the Downeyite structure ($P4_2/mbc$, $Z = 8$, α-SeO_2 stable at ambient conditions) as well as in the β-SeO_2 and γ-SeO_2 phases are indeed found also in all lowest-enthalpy phases of SO_2 at high-pressure. However, we found that the Downeyite-like stacking of the chains is far from favourable for high-pressure SO_2. We structurally optimized the Downeyite-like SO_2 at 40 GPa (Fig.S7 in Supp. Mat.) and found that its enthalpy is higher by 0.32 eV per f.u. than the best γ-SeO_2-like phase, much above all phases we considered. Also, we note that the stacking in the *Ama*2 phase (all chains with the same orientation) is not known in SeO_2. The polymeric SO_2 phases stable above 25 GPa correspond to the γ and β-SeO_2 phases which are stable at pressure above 6 GPa and 2 GPa and temperature above and below 600 K, respectively[40]. The high-pressure polymeric structures of SO_2 are thus closely related or identical to the low-pressure structures of SeO_2, but less similar to the ambient pressure form of SeO_2.

Comparison of experimental observations to DFT simulations: identification of a SO_2 W-shaped polymer

To determine the conformation and structure of polymeric SO_2, we computed X-ray diffraction patterns and simulated Raman/IR spectra for the candidate structures discussed earlier (see Methods for details). Comparison of the predicted low-enthalpy structures with experimental Raman spectra and XRD patterns (Supplementary Figs. S3, S4) demonstrates a qualitative agreement with the energetically competitive structures consisting of W-shaped polymers. A conformational fingerprint, which appears in all four W-polymer candidate structures (γ-SeO_2-like $Pmc2_1$, β-SeO_2-like $Pmc2_1$, *Ama*2, and *Pm* phases), is the large frequency gap between double-bond S=O_T stretches (1200–1300 cm^{-1}) and single-bond S-O_B modes (600–900 cm^{-1}). This gap, also experimentally observed in polymeric SeO_2[40], confirms the polymeric nature, though DFT slightly underestimates its magnitude in polymeric SO_2[38], likely due to limitations in the functionals used. Initial LDA-calculated Raman spectra (Figs. S3, 4; LDA was used because of the Quantum Espresso constraints) required a +97 cm^{-1} shift for S=O_T modes to match experiment (Fig. 5(b), inset). However, SCAN functional calculations[47] reduced this discrepancy significantly, with S=O_T frequencies shifting upward by 40–50 cm^{-1} and yielding better agreement with experimental data. The two predicted stable polymeric phases, *Ama*2 and γ-SeO_2-like $Pmc2_1$, exhibit nearly degenerate enthalpies at 25 GPa (see Fig. 4), precisely where we observe the onset of polymerization. Their enthalpies, remain close across a broad pressure range surrounding this transition, while the two metastable phases (β-SeO_2-like $Pmc2_1$ and *Pm*) show similarly small energy differences. This energetic degeneracy strongly suggests the coexistence of multiple phases is not only possible but thermodynamically favoured. We therefore proceed with our analysis under the assumption that both *Ama*2 and γ-SeO_2-like $Pmc2_1$ phases are present in our samples.

The crystalline nature of polymeric SO_2 is unequivocally demonstrated by the sharp Bragg peaks in the X-ray diffraction pattern of a bulk sample at 54 GPa (Figs. S4 and Fig. 5(c)), consistent with optical spectra in Figs. 1(a), 2, 5(a), and S3. This contrasts markedly with amorphous polymeric SO_2, which shows only broad, diffuse peaks due to the absence of long-range order[33] (Fig. S1). While Raman spectra reveal minor amorphous contributions (starred features in Fig. 1(a)), these are negligible compared to the dominant crystalline signal in diffraction measurements. The crystalline nature of the sample allows us not only access to the thermodynamically favourable state of the SO_2 at these conditions,

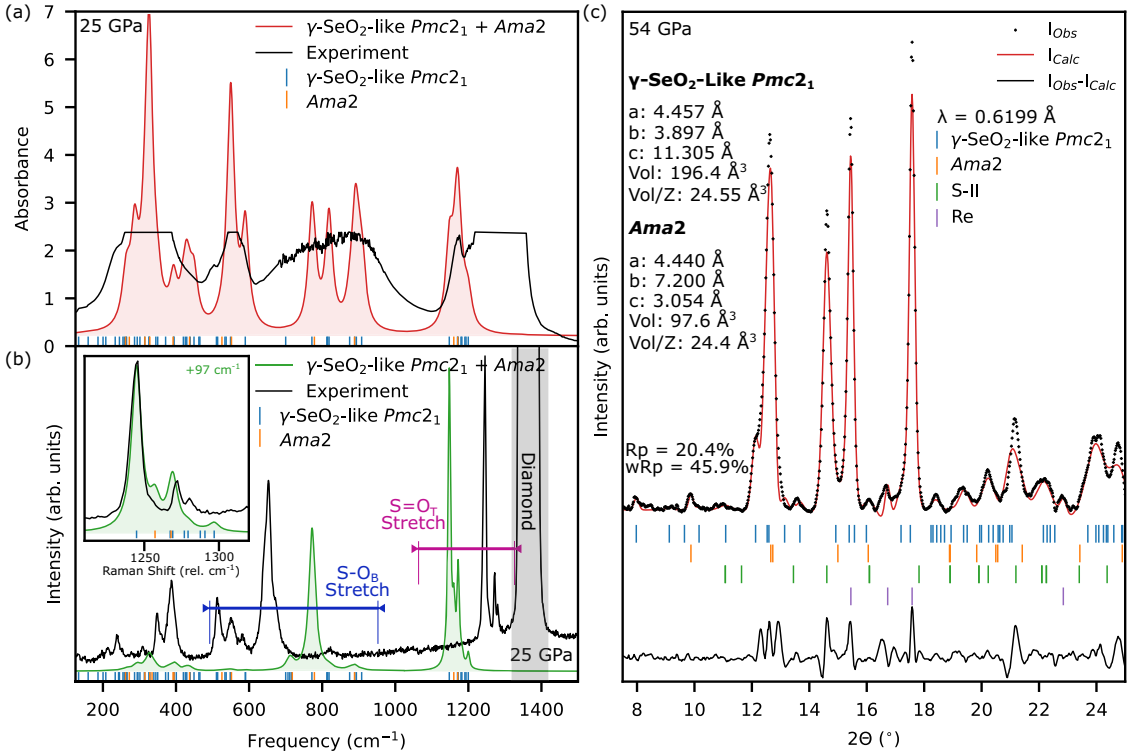

Fig. 5 | Comparison of experimentally measured polymeric SO_2 with DFT simulations of candidate γ-SeO_2-like $Pmc2_1$ and $Ama2$ mixtures. a–c present complementary techniques: **a** Far and mid-infrared synchrotron absorption measurements of bulk polymeric SO_2 decompressed from 50 GPa to 25 GPa. **b** Raman spectrum of polymeric SO_2 synthesized in an O_2-He mixture, that is also measured at 25 GPa after decompression from 50 GPa (inset is simulated Raman spectrum and frequencies shifted for a direct comparison of $S{=}O_T$ vibrational modes) and (**c**) Le Bail refinement of synchrotron X-ray diffraction data from bulk polymeric SO_2 collected at 54 GPa on compression.

but also to assess the packing and arrangement of the W-shaped polymers. The agreement between experimental and simulated patterns for both γ-SeO_2-like $Pmc2_1$ and $Ama2$ structures provides compelling evidence for the structural arrangement of the W-shaped polymeric units. Key features are well reproduced: (i) the γ-SeO_2-like phase accounts for strong reflections at ~12. 5° (with shoulder at ~12°) and the ~8° peak (Fig. 5(c)), while (ii) $Ama2$ is essential to explain the ~9.75° peak and ~13° reflection asymmetry. A Le Bail refinement accounting for this phase mixture at 55 GPa, Fig. 5(c), yields lattice parameters in good agreement with DFT predictions: γ-SeO_2-like $Pmc2_1$ $a = 4.457$ Å ($a_{DFT} = 4.4352$ Å), $b = 3.897$ Å ($b_{DFT} = 3.9075$ Å), $c = 11.305$ Å ($c_{DFT} = 11.2529$ Å) and $Ama2$ $a = 4.440$ Å ($a_{DFT} = 4.4345$ Å), $b = 7.200$ Å ($b_{DFT} = 7.2021$ Å), $c = 3.054$ Å ($c_{DFT} = 3.0568$ Å). The largest discrepancy being 0.5% in the a-lattice parameter for the γ-SeO_2-like $Pmc2_1$ and can be due to broad peaks and closely-spaced reflections. The refinement also accounts for minor rhenium (gasket) and sulfur-II impurities, the latter arising from X-ray induced decomposition (evident optically from sample darkening). Similar results at 48 GPa (Fig. S5) and another X-ray wavelength, further support the structural assignment and mixture of γ-SeO_2-like $Pmc2_1$ and $Ama2$ phases. Despite sharp Raman features indicating high crystallinity, single-crystal diffraction of He-synthesized samples (Method II) proved unsuccessful due to the strain-induced peak broadening, an example of the non-ideal peak shape can be seen in Fig. S6. This reflects the material's mechanical softness, where minor deviatoric stresses degrade diffraction quality despite the well-defined local structure of the W-shaped polymers.

The observed Raman and infrared activity of polymeric SO_2 at 25 GPa are also compatible with the proposed γ-SeO_2-like $Pmc2_1$-$Ama2$ mixture, as shown in Fig. 5(c), which have been evidenced from numerical simulations and diffraction experiments. Notably, there are two key regions to evaluate the candidacy of the low-enthalpy structures: the $S{=}O_T$ region (~1000–1300 cm^{-1}) and the $S{-}O_B$ region (~500–900 cm^{-1}). Remarkably, the Raman spectral signature of polymeric SO_2 observed in this study is strikingly similar to that of polymeric homologue SeO_2, which is known to exist in multiple crystalline arrangements, including both γ-SeO_2-like $Pmc2_1$ and β-SeO_2-like $Pmc2_1$ at higher pressures and temperatures[40]. In the $S{=}O_T$ region at 25 GPa, it is evident that both the γ-SeO_2-like $Pmc2_1$ and $Ama2$ phases must be present to accurately account for the numerous Raman actives mode in this region, seen in Fig. 5(b) and Fig. S3. Further, as seen from infrared absorption measurements a combination of $Ama2$ and $Pmc2_1$ are found to accurately describe the broad region of infrared activity 600–1100 cm^{-1} associated to the newly formed $S{-}O_B$ vibrational modes of the polymer. Finally, given that the $Ama2$, γ-SeO_2-like $Pmc2_1$ and β-SeO_2-like $Pmc2_1$ (at higher pressures) structures are energetically competitive and can mix at a minimal energy cost, the observed peak splittings and disorder-activated modes may account for additional contributions seen in the experimentally observed spectra and can result in a more complicated spectrum at the highest pressures, seen in Fig. 1(b, c).

Conclusion

The nature of pressure-induced polymerisation of SO_2 has been explored and characterized using XRD, Raman spectroscopy, infrared spectroscopy and ab initio simulations up to 55 GPa. We present a methodology for producing highly crystalline polymeric samples, which can be particularly challenging due to the polymerisation process under compression and is crucial for systems where conventional sample annealing techniques are unsuitable. Through Raman and infrared diagnostics, the molecular-to-polymeric transition was mapped at room temperature and was found to initiate upon compression at 21 GPa, and with the polymer being recoverable to 17 GPa on decompression, indicative of hysteresis resulting from the chemical changes. Extensive random structure and metadynamics searches involving up to eight SO_2 molecules yielded four distinct polymeric

candidate structures: *Pm*, $Pmc2_1$ ($Z = 4$, β-SeO_2-like), *Ama*2, $Pmc2_1$ ($Z = 8$, γ-SeO_2-like). Notably, the competitive structures are polytypes consisting of efficiently-packed W-shaped polymeric chains, a structural motif previously identified at ambient pressure only in the rare-mineral Downeyite (SeO_2). *Ama*2 and $Pmc2_1$ ($Z = 8$, γ-SeO_2-like) were the most energetically competitive and found to be degenerate at 25 GPa, the experimentally observed onset pressure for polymerization, suggesting that a mixture of structures should be expected. Powder XRD measurements and Le Bail fits revealed that a combination of *Ama*2 and γ-SeO_2-like phases could describe the observed Bragg reflections, substantiating the structural assignment. DFT simulated vibrational activities showed qualitative agreement with all W-shaped polymers, with the experimentally observed Raman and IR activities well described by the low-enthalpy structural candidates *Ama*2 and γ-SeO_2-like accounting for observed vibrational excitations. We have then demonstrated that, at the high-pressures, SO_2 is thermodynamically stable as a crystal polymer, whereas the amorphous polymer previously found[33] is metastable like all amorphous solids. Last but not least, the similarity between polymeric SO_2 and a selenium dioxide mineral represents a nontrivial case of homologous chemical behaviour between light and heavy elements of the same group, under appropriate density conditions.

Methods

Experimental methods

Experiments were conducted using symmetric diamond anvil cells (DACs) equipped with type-IIas diamonds. Diamonds with 200 μm culets were utilized, allowing for routine pressures of up to 50 GPa without damage. Sample containment was provided by a rhenium gasket, a material known for its strong chemical resistance, featuring a laser-machined cavity with initial dimensions dependent on the loading procedure. During these experiments, pressure was determined using either the fluorescence of a ruby sphere[48] or the Raman-active phonon of the diamond anvil[49].

Loading procedures for SO_2. **Method 1:** Bulk SO_2 (99.9%) was loaded as a liquid at >1.6 bars and 0 °C using a pressure chamber that was purged several times prior to loading, and submerged in an ice/water bath. Due to the reactivity and hygroscopic nature of SO_2, all samples were screened with Raman and IR measurements to ensure purity. To minimize shear-induced amorphisation of SO_2[33], sample deformation was reduced by using smaller initial gasket dimensions, typically around 50 μm in diameter and 20 μm in thickness. This resulted in a homogeneous bulk sample of reasonable crystalline quality upon compression into the polymeric phase. All infrared spectroscopic measurements in this study used this loading methodology for SO_2.

Method 2: SO_2 was synthesized in situ by direct reaction between sulphur (S) and a high-purity gaseous mixture of O_2 (1–10%) with helium (He) as the balance at a pressure of 0.17 GPa. A grain of sulphur was loaded into the DAC, and initial sample chambers were designed to be larger, typically around 100 μm in diameter and 35 μm in thickness, to accommodate for the large compressibility of helium. The pressure was increased until the sulphur strongly absorbed 532 nm light, approximately at 1–2 GPa. The direct reaction between sulphur and the surrounding oxygen gas was initiated by irradiating the sulphur with focused 532 nm laser light at a high energy density of ~30 mW/μm^2. This synthesis procedure produced SO_2 samples of superior crystalline quality, as evidenced by sharp Raman peaks (see Fig. 1(b, c). In many cases, similar high-pressure synthesis of compounds directly from the elements has been obtained, for example in the systems H-S, H-Se, and H-S-Se[50–54].

Raman spectroscopy. Raman experiments were performed using a custom micro-focused confocal optical system. Raman scattering was excited using both 532 nm and 660 nm wavelengths with a spot size of approximately 2 μm. To avoid unwanted sample heating or possible photochemistry during measurements, the incident laser power was maintained below 5 mW for both excitation wavelengths. The back-scattered light was collected and filtered through ultra-narrow notch filters, then dispersed by an aberration-corrected spectrometer and imaged using a liquid nitrogen-cooled CCD detector.

Far/Mid-IR transmission and reflectivity measurements. In-house mid-IR reflectivity measurements were conducted using a Bruker Vertex 70v FT-IR interferometer with a Globar source and a KBr beamsplitter. The mid-IR transmission was focused and captured using a pair of x15 (0.4 NA) Schwarzschild objectives and a liquid nitrogen-cooled mercury cadmium telluride (MCT) detector. All acquisitions comprised 300 scans with a resolution of 2 cm^{-1}. Partial reflectance was calculated taking the ratio of the MIR spectra of the SO_2-sample and surrounding rhenium gasket, (I_{SO2}/I_{Re}), at every pressure point.

Synchrotron far-infrared (FIR) and mid-infrared (MIR) transmission measurements were carried out on the horizontal microscope of the SMIS beamline at the SOLEIL synchrotron. The synchrotron IR radiation was focused on the DAC by a couple of custom Schwarzschild objectives (NA=0.5). Spectra were collected by a ThermoFisher iS50 FTIR spectrometer, equipped with a Liquid He cooled Si bolometer and a solid substrate beamsplitter for the FIR range, whereas a MCT detector and a KBr beamsplitter are used for the MIR range. Spectral resolution is set to 2 cm^{-1}. To compute the absorbance, a reference was taken with the empty cell with the diamond anvils in contact, to reduce interference fringes.

X-ray diffraction. X-ray diffraction was performed at the nanoMAX beamline (ID27 beam line) at MAX IV in Sweden (ESRF in France). The incident X-ray spot had a wavelength of 0.6199 Å and a diameter of approximately 0.1 μm (0.3738 Å and 0.5 μm for ID27-ESRF). The resultant diffraction pattern was imaged using the Eiger2 CdTe 9M detector, and the data were integrated into a 1D format using Dioptas software[55]. Le Bail refinements were conducted using the Jana software package[56].

Simulation methods

For crystal structure search we used the random search method[41] as implemented in the CRYSPY package[57]. Ab initio calculations (structure optimizations in random search and MD simulations in metadynamics simulations) were performed by the VASP package[58,59] employing PAW pseudopotentials[60] and the PBE exchange-correlation functional[42]. For the enthalpy calculations we employed the r^2SCAN+rVV10[45] functional and hard pseudopotentials S_h and O_h from the VASP library with a cutoff of 910 eV. Metadynamics simulations employing the supercell as collective variable were performed with the approach described in refs. 43,44. Phonon calculations including calculation of infrared and Raman cross sections were performed by the Quantum Espresso package[61,62] employing the LDA exchange-correlation functional[63,64] and norm-conserved pseudopotentials[65] with a cutoff of 100 Ry. For the simulated Raman spectra, Lorentzian peaks are built upon the obtained cross-sections and frequencies using widths (FWHM) reflecting experimental observations, 4 cm^{-1} and 10 cm^{-1} for S=O_T and S-O_B, respectively. For Infrared simulated spectra, Lorentzian peaks are all assigned a width of 10 cm^{-1} as due to saturation, experimentally observed peak FHWMs could not be extracted. Diffraction patterns of candidate structures were calculated using the VESTA software package[66].

Data availability

The data that support the findings of this study are available on request from the authors.

Code availability

The code used to support the findings of this study are available on request from the authors.

Received: 26 February 2025; Accepted: 17 October 2025;
Published online: 26 November 2025

References

1. Sauer, G. E. & Borst, L. B. Lambda transition in liquid sulfur. *Science* **158**, 1567–1569 (1967).
2. Henry, L. et al. Liquid-liquid transition and critical point in sulfur. *Nat. 2020 584:7821* **584**, 382–386 (2020).
3. Sun, J., Martinez-Canales, M., Klug, D. D., Pickard, C. J. & Needs, R. J. Persistence and eventual demise of oxygen molecules at terapascal pressures. *Phys. Rev. Lett.* **108**, 045503 (2012).
4. Martin, R. M. & Needs, R. J. Theoretical study of the molecular-to-nonmolecular transformation of nitrogen at high pressures. *Phys. Rev. B* **34**, 5082–5092 (1986).
5. Goncharov, A. F., Gregoryanz, E., Mao, H. K., Liu, Z. & Hemley, Ru. J. Optical evidence for a nonmolecular phase of nitrogen above 150 GPa. *Phys. Rev. Lett.* **85**, 1262–1265 (2000).
6. Eremets, M. I., Hemley, R. J., Mao, H. K. & Gregoryanz, E. Semiconducting non-molecular nitrogen up to 240 GPa and its low-pressure stability. *Nature* **411**, 170–174 (2001).
7. Gregoryanz, E., Goncharov, A. F., Hemley, R. J. & Mao, H. K. High-pressure amorphous nitrogen. *Phys. Rev. B* **64**, 052103 (2001).
8. Eremets, M. I. et al. Structural transformation of molecular nitrogen to a single-bonded atomic state at high pressures. *J. Chem. Phys.* **121**, 11296–11300 (2004).
9. Plašienka, D. & Martoňák, R. Transformation pathways in high-pressure solid nitrogen: from molecular N_2 to polymeric cg-N. *J. Chem. Phys.* **142**, 094505 (2015).
10. Melicherová, D., Kohulák, O., Plašienka, Dcv & Martoňák, R. Structural evolution of amorphous polymeric nitrogen from ab initio molecular dynamics simulations and evolutionary search. *Phys. Rev. Mater.* **2**, 103601 (2018).
11. Melicherová, D. & Martoňák, R. Study of polymerization of high-pressure nitrogen by ab initio molecular dynamics. *J. Chem. Phys.* **158**, 244503 (2023).
12. Katz, A. I., Schiferl, D. & Mills, R. L. New phases and chemical reactions in solid carbon monoxide under pressure. *J. Phys. Chem.* **88**, 3176–3179 (1984).
13. Lipp, M. J., Evans, W. J., Baer, B. J. & Yoo, C.-S. High-energy-density extended CO solid. *Nat. Mater.* **4**, 211–215 (2005).
14. Bernard, S., Chiarotti, G. L., Scandolo, S. & Tosatti, E. Decomposition and polymerization of solid carbon monoxide under pressure. *Phys. Rev. Lett.* **81**, 2092–2095 (1998).
15. Sun, J., Klug, D. D., Pickard, C. J. & Needs, R. J. Controlling the bonding and band gaps of solid carbon monoxide with pressure. *Phys. Rev. Lett.* **106**, 145502 (2011).
16. Santoro, M. et al. High pressure structural changes in amorphous polymeric carbon monoxide by combined infrared spectroscopy and X-ray diffraction. *J. Phys. Chem. C* **126**, 11840 - 11845 (2022).
17. Iota, V., Yoo, C. S. & Cynn, H. Quartzlike carbon dioxide: an optically nonlinear extended solid at high pressures and temperatures. *Science* **283**, 1510–1513 (1999).
18. Sun, J. et al. High-pressure polymeric phases of carbon dioxide. *Proc. Natl. Acad. Sci.* **106**, 6077–6081 (2009).
19. Datchi, F., Mallick, B., Salamat, A. & Ninet, S. Structure of polymeric carbon dioxide CO_2-V. *Phys. Rev. Lett.* **108**, 125701 (2012).
20. Santoro, M. et al. Partially collapsed cristobalite structure in the non molecular phase V in CO_2. *Proc. Natl. Acad. Sci.* **109**, 5176–5179 (2012).
21. Bridgman, P. W. Freezing parameters and compressions of twenty-one substances to 50,000 kg/cm^2. *Proc. Am. Acad. Arts Sci.* **74**, 399–424 (1942).
22. Whalley, E. Structure of Bridgman's black carbon disulphide. *Can. J. Chem.* **38**, 2105–2108 (1960).
23. Dias, R. P., Yoo, C.-S., Kim, M. & Tse, J. S. Insulator-metal transition of highly compressed carbon disulfide. *Phys. Rev. B* **84**, 144104 (2011).
24. Naghavi, S. S., Crespo, Y., Martoňák, R. & Tosatti, E. High-pressure layered structure of carbon disulfide. *Phys. Rev. B* **91**, 224108 (2015).
25. Zarifi, N., Liu, H. & Tse, J. S. Structures of the metallic and superconducting high pressure phases of solid CS2. *Sci. Rep.* **5**. https://doi.org/10.1038/srep10458 (2015).
26. Yan, J. et al. High-pressure structural evolution of disordered polymeric CS_2. *J. Phys. Chem. Lett.* **12**, 7229–7235 (2021).
27. Cansell, F., Fabre, D. & Petitet, J. Phase transitions and chemical transformations of benzene up to 550 °C and 30 GPa. *J. Chem. Phys.* **99**, 7300–7304 (1993).
28. Ciabini, L., Santoro, M., Bini, R. & Schettino, V. High pressure photoinduced ring opening of benzene. *Phys. Rev. Lett.* **88**, 085505 (2002).
29. McCullough, J. D. The crystal structure of selenium dioxide. *J. Am. Chem. Soc.* **59**, 789–794 (1937).
30. Laniel, D., Geneste, G., Weck, G., Mezouar, M. & Loubeyre, P. Hexagonal layered polymeric nitrogen phase synthesized near 250 GPa. *Phys. Rev. Lett.* **122**, 066001 (2019).
31. Eremets, M., Gavriliuk, A., Trojan, I. A., Dzivenko, D. A. & Boehler, R. Single-bonded cubic form of nitrogen. *Nat. Mater.* **3**, 558–563 (2004).
32. Santoro, M. et al. Amorphous silica-like carbon dioxide. *Nature* **441**, 857 - 860 (2006).
33. Zhang, H. et al. Pressure-induced amorphization and existence of molecular and polymeric amorphous forms in dense SO_2. *Proc. Natl. Acad. Sci.* **117**, 8736–8742 (2020).
34. Vandaele, A. C. et al. Sulfur dioxide in the Venus atmosphere: I. vertical distribution and variability. *ICARUS* **295**, 16–33 (2017).
35. Post, B., Schwartz, R. S. & Fankuchen, I. The crystal structure of sulfur dioxide. *Acta Crystallogr.* **5**, 372–374 (1952).
36. Swanson, B. I. et al. Raman study of SO2 at high pressure: aggregation, phase transformations, and photochemistry. *Chem. Phys. Lett.* **91**, 393–395 (1982).
37. Song, Y., Liu, Z., Mao, H., Hemley, R. J. & Herschbach, D. R. High-pressure vibrational spectroscopy of sulfur dioxide. *J. Chem. Phys.* **122**, 174511 (2005).
38. Lu, W. et al. Disproportionation of SO_2 at high pressure and temperature. *Phys. Rev. Lett.* **128**, 106001 (2022).
39. Finkelman, R. B. & Mrose, M. E. Downeyite, the first verified natural occurrence of seo2. *Am. Mineralog.* **62**, 316–320 (1977).
40. Orosel, D., Leynaud, O., Balog, P. & Jansen, M. Pressure-temperature phase diagram of SeO_2. Characterization of new phases. *J. Solid State Chem.* **177**, 1631–1638 (2004).
41. Pickard, C. J. & Needs, R. J. High-pressure phases of silane. *Phys. Rev. Lett.* **97**, 045504 (2006).
42. Perdew, J. P., Burke, K. & Ernzerhof, M. Generalized gradient approximation made simple. *Phys. Rev. Lett.* **77**, 3865–3868 (1996).
43. Martoňák, R., Laio, A. & Parrinello, M. Predicting crystal structures: the Parrinello-Rahman method revisited. *Phys. Rev. Lett.* **90**, 075503 (2003).
44. Martoňák, R., Donadio, D., Oganov, A. R. & Parrinello, M. Crystal structure transformations in SiO_2 from classical and ab initio metadynamics. *Nat. Mater.* **5**, 623–626 (2006).
45. Ning, J. et al. Workhorse minimally empirical dispersion-corrected density functional with tests for weakly bound systems: r^{2}SCAN+rVV10. *Phys. Rev. B* **106**, 075422 (2022).
46. Kothakonda, M. et al. Testing the r^{2}SCAN density functional for the thermodynamic stability of solids with and without a van der Waals correction. *ACS Mater. Au* **3**, 102–111 (2023).
47. Sun, J., Ruzsinszky, A. & Perdew, J. P. Strongly constrained and appropriately normed semilocal density functional. *Phys. Rev. Lett.* **115**, 036402 (2015).
48. Shen, G. et al. Toward an international practical pressure scale: a proposal for an IPPS ruby gauge (IPPS-Ruby2020). *High Press. Res.* 299–314. https://doi.org/10.1080/08957959.2020.1791107 (2020).
49. Akahama, Y. & Kawamura, H. Pressure calibration of diamond anvil Raman gauge to 310 GPa. *J. Appl. Phys.* **100**, 043516 (2006).

50. Pace, E. J. et al. Synthesis and stability of hydrogen selenide compounds at high pressure. *J. Chem. Phys.* **147**, 184303 (2017).
51. Guigue, B., Marizy, A. & Loubeyre, P. Direct synthesis of pure H_3S from S and H elements: no evidence of the cubic superconducting phase up to 160 GPa. *Phys. Rev. B* **95**, 020104 (2017).
52. Goncharov, A. F., Lobanov, S. S., Prakapenka, V. B. & Greenberg, E. Stable high-pressure phases in the H-S system determined by chemically reacting hydrogen and sulfur. *Phys.Rev. B* **95**, 140101 (2017).
53. Pace, E. J. et al. Properties and phase diagram of $(H_2S)_2H_2$. *Phys. Rev. B* **101**, 174511 (2020).
54. Pena-Alvarez, M. et al. Pressure-induced synthesis and properties of an H_2S-H_2Se-H_2 molecular alloy. *J. Phys. Chem. Lett.* **12**, 5738–5743 (2021).
55. Prescher, C. & Prakapenka, V. B. Dioptas: a program for reduction of two-dimensional X-ray diffraction data and data exploration. *High. Press. Res.* **35**, 223–230 (2015).
56. & Petříček, V. Jana 2020—a new version of the crystallographic computing system Jana. *Z. fur Kristallogr.- Cryst. Mater.* **238**, 271–282 (2023).
57. Yamashita, T. et al. Cryspy: a crystal structure prediction tool accelerated by machine learning. *Sci. Technol. Adv. Mater.: Methods* **1**, 87–97 (2021).
58. Kresse, G. & Furthmüller, J. Efficient iterative schemes for ab initio total-energy calculations using a plane-wave basis set. *Phys. Rev. B* **54**, 11169–11186 (1996).
59. Kresse, G. & Furthmüller, J. Efficiency of ab-initio total energy calculations for metals and semiconductors using a plane-wave basis set. *Comput. Mater. Sci.* **6**, 15–50 (1996).
60. Kresse, G. & Joubert, D. From ultrasoft pseudopotentials to the projector augmented-wave method. *Phys. Rev. B* **59**, 1758–1775 (1999).
61. Giannozzi, P. et al. Quantum espresso: a modular and open-source software project for quantum simulations of materials. *J. Phys. Condens. Matter* **21**, 395502 (2009).
62. Giannozzi, P. et al. Advanced capabilities for materials modelling with Quantum Espresso. *J. Phys. Condens. Matter* **29**, 465901 (2017).
63. Ceperley, D. M. & Alder, B. J. Ground state of the electron gas by a stochastic method. *Phys. Rev. Lett.* **45**, 566–569 (1980).
64. Perdew, J. P. & Zunger, A. Self-interaction correction to density-functional approximations for many-electron systems. *Phys. Rev. B* **23**, 5048–5079 (1981).
65. We used the pseudopotentials O.pw-mt_fhi.UPF and S.pw-mt_fhi.UPF from https://www.quantum-espresso.org.
66. Momma, K. & Izumi, F. *V*ESTA3 for three-dimensional visualization of crystal, volumetric and morphology data. *J. Appl. Crystallogr.* **44**, 1272–1276 (2011).

Acknowledgements

This work was supported by the Slovak Research and Development Agency (Contracts nos. APVV-19-0371 and APVV-23-0515) and the National Natural Science Foundation of China (NSFC grant number W2532012). We acknowledge MAX IV Laboratory for time on Beamline NanoMAX under Proposal 20210122. Research conducted at MAX IV, a Swedish national user facility, is supported by the Swedish Research council under contract 2018-07152, the Swedish Governmental Agency for Innovation Systems under contract 2018-04969, and Formas under contract 2019-02496. We also acknowledge the European Synchrotron Radiation Facility (ESRF) for provision of beam time at the ID27 beam line. M. S. acknowledges HPSTAR for having allowed him as a Visiting Scientist during part of his research on SO_2.

Author contributions

P.D-S., M.S., F.A.G. and R.M. conceived the experiment(s), H.Z., P.D-S., F.C., M.S. and F.A.G. conducted the Raman and Infrared experiment(s), where H.Z., P.D-S., M.S., F.A.G. and R.M. analysed the results. H.Z., J.C., L.Z., P.D-S. and F.A.G. carried out diffraction measurements and its subsequent analysis. R.M. conducted ab initio crystal search and metadynamics simulations as well as calculations of Raman and Infrared spectra. P. D-S., M. S., F.A.G. and R.M. wrote the paper. All authors reviewed the manuscript.

Competing interests

The authors declare no competing interests.

Additional information

Supplementary information The online version contains supplementary material available at https://doi.org/10.1038/s42004-025-01757-y.

Correspondence and requests for materials should be addressed to Philip Dalladay-Simpson, Mario Santoro, Federico A. Gorelli or Roman Martoňák.

Peer review information *Communications Chemistry* thanks Xiao Dong and the other, anonymous, reviewers for their contribution to the peer review of this work.